INVESTIGATING BEHAVIORAL DYNAMICS WITH A FIXED-TIME EXTINCTION SCHEDULE AND LINEAR ANALYSIS

WILLIAM L. PALYA, DON WALTER, ROBERT KESSEL, AND ROBERT LUCKE

JACKSONVILLE STATE UNIVERSITY AND NAVAL RESEARCH LABORATORY

This paper describes the behavioral adaptation observed for 16 pigeons responding to a step transition in the reinforcement rate in a repeated-trial design. Within each trial, following exposure for a fixed period to a variable-interval schedule, there was an unsignaled change in the schedule to extinction. The step transition allowed an experimental test of the applicability of a linear analysis to steady-state dynamic behavior. The computations required for this test yielded, as an intermediate result, transfer functions for each of the 16 birds from 1 mHz to 256 mHz. The transfer functions obtained show greater responsiveness to lower frequencies (i.e., longer time-scale structures in the reinforcement schedule); hence, the pigeons have the characteristics of a low-pass filter. The outcome of the test is that some predictability of the pigeons' future behavior is possible.

Key words: linear systems analysis, frequency domain, variable-interval schedules, transfer function, interreinforcement interval distribution, key peck, pigeons

---

Ultimately, our goal for behavior analysis is to predict fully the behavior that will be supported by any given environment. The endpoint of our report's data reduction is a χ_v^2 assessment of a prediction of steady-state dynamic behavior made by linear analysis. In the course of this report, we will develop the techniques used for the predictions and obtain some useful intermediate results.

Over the past few decades, environmental input and the supported behavior have often been characterized with globally time-averaged parameters. Typically, reinforcement schedule data from an entire session, or several sessions, are combined to yield a single parameter such as average rate of reinforcement or average ratio of reinforcers between the alternatives of a concurrent schedule. Similarly, long samples of the supported behavioral output are compressed into a parameter such as average responses per second or average ratio of responding to the alternatives of a concurrent schedule. This has been a fruitful approach and has led to quantitative molar predictions for the dependence of global time average response rates upon global time average schedule parameters. For at least some schedules, these relationships are reasonably well established (e.g., the generalized matching law, Baum, 1979). The moment-to-moment structure of behavior seen in response to a dynamic (i.e., time varying) input, even in average steady state, has received less attention.

Galbicka, Kautz, and Jagers (1993) and Galbicka (in press) suggest that the analysis of behavior be broadened well beyond contingencies that are designed to minimize local variation in response structure (e.g., constant-probability variable-interval schedules). The present report focuses on the steady-state behavioral adaptation supported by an unsignaled step transition in the contingencies of reinforcement and on describing this adaptation with a linear analysis (McDowell, Bass, & Kessel, 1993). This focus on the steady-state behavior supported by a schedule transition in repeated trials provides an intermediate step between completely local, or molecular, measurements of a unique behavioral occur-

rence and global, or molar, time averages of behavior across multiple sessions.

This experiment has a very simple dynamic structure as part of the reinforcement contingency: a step transition from a variable-interval (VI) schedule to extinction. Like a mixed schedule, the procedure repetitively switched between a VI schedule and extinction with no change in the explicit stimuli. The task of the present research is not simply to determine if pigeons peck during the period when the reinforcer is available and refrain from pecking during extinction. Rather, our task is to quantify the relation between this dynamic reinforcement schedule and the supported behavior using a construct from linear analysis called a *transfer function.* (Note that linear analysis, by itself, does not determine what schedule will be the most useful in an initial study of behavioral dynamics.) McDowell, Bass, and Kessel (1992) showed that if the transfer function (or linear kernel) were known, then the dynamic behavior supported by a step transition between two VI schedules could be computed. Of course, at present, the transfer function is not known a priori; instead, it must be measured experimentally: If the average moment-to-moment behavior generated by a particular step transition is measured, then a computational technique exists that combines the reinforcement schedule with the behavioral data to determine the transfer function. Once an organism's transfer function is extracted using one reinforcement input/behavior output pair, its behavior for a new reinforcement schedule can be predicted based solely on this transfer function and the new schedule. The more closely the predicted behavior agrees with the measured behavior, the more useful a linear analysis will be in understanding the relation between the reinforcement schedule and supported behavior. Because this is the first use of a linear analysis with time-dependent behavioral data, a major portion of this paper is, accordingly, a presentation of the analytic and numerical techniques involved.

The report begins with the traditional description of the experimental method. The next section then develops the general method and auxiliary techniques we use to make a prediction of behavior. The first portion of this section is an averaging method that is used to combine data from the repeated trials. The second part is an introduction to Fourier transforms (a standard technique of linear analysis). The third subsection is a long thoroughgoing discussion of the method used to extract a transfer function from data and predict behavior under a new schedule. There are two parts in the results section. First, we show, for 1 bird, all of the intermediate results obtained in the process of determining the transfer function and predicting the output given a novel input. In the second part of the results section we define the appropriate reduced χ^2 test and then assess the predictions' fidelity to the observed behavior on the new schedule for the remaining 15 birds. The paper concludes with a brief discussion section. There is also an Appendix that covers some relevant technical aspects of linear analysis.

METHOD

Subjects

Sixteen adult experimentally naive pigeons obtained from a local supplier were used. They were housed under a 19:5 hr light/dark cycle in individual cages with free access to water. All were maintained at approximately 80% of their ad lib weights by limited feeding with pelletized laying mash.

Apparatus

Five experimental chambers were used. The interior of each was a box (30 cm by 30 cm by 34 cm high). An unfinished aluminum panel served as one wall of the chamber; the other sides were painted white. The stimulus panel had a feeder aperture 5 cm in diameter, medially located 10 cm above the grid floor. Three response keys, each 2 cm in diameter, were located 9 cm apart, 29 cm above the grid floor. Only the center key was used. It required approximately 0.15 N to operate. The key was transilluminated by a stimulus projector containing the Rosco pea (86, yellow green) theatrical gel throughout all phases of the experiment, with the exception of the scheduled blackouts and during reinforcement. Two houselights were located on the stimulus panel 32 cm above the grid floor. The lamps were shielded such that their light was directed towards the ceiling. Ventilation was provided by an exhaust fan mounted on the outside of the chamber. A white noise
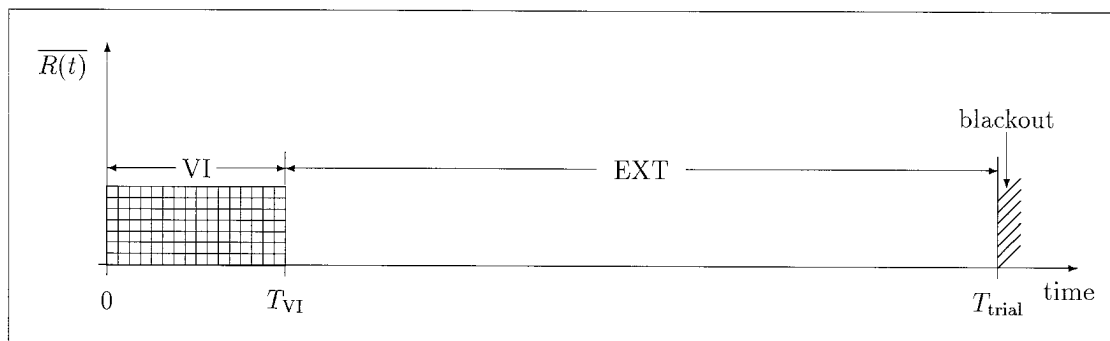
Fig. 1. A schematic of the basic procedure used for the transition trials of this experiment. The time intervals used are T_{trial} = 1,000 s, a 10-s chamber blackout, and T_{VI} = 200 s or 300 s. $\overline{R(t)}$ is the locally averaged reinforcement rate.

generator provided ambient masking noise in the chamber. Stimulus events were controlled and key pecks were recorded by a computer system (Palya & Walter, 1993). The computer archived the time of each stimulus and response event in 1-ms "ticks." Subsequent data extraction and analysis routines provided the derived data. Complete raw data event logs of all research are maintained for 10 years and are available from the authors.

Procedure

All pigeons were magazine trained to approach and eat from the food magazine within 3 s on three consecutive presentations. The birds were then autoshaped to peck the center key, and subsequent responding was maintained under a short VI schedule in the presence of the pea-colored keylight. To maintain a constant weight throughout the course of the experiment, each session typically contained 45 to 55 food presentations, the exact number being determined by the bird's body weight that day. Experimental treatments (phases) were continued until there were no apparent session-to-session trends in the data, as judged by visually inspecting daily plots of behavioral measures.

The data came from two VI-to-extinction step-transition schedules (Phases 1 and 2). The step-transition procedure is illustrated in Figure 1. Within each trial, the pigeons were first exposed to a VI schedule for a period T_{VI}. Next, an unsignaled transition to extinction occurred. There were no changes in any explicit stimuli. Extinction was in effect from T_{VI} to T_{trial}. The only stimulus correlated with the step transition was the consistent tempo-

ral duration of T_{VI}. The end of the extinction period was followed by a 10-s blackout, during which the chamber was totally dark. This blackout procedure provided a relatively sharp demarcation at the beginning of each trial. The chamber was also dark for several seconds between the time the birds were first put in the chamber and the time the control software started a session's first trial. There were typically five step-transition trials in each session.

Any initial study of steady-state behavioral dynamics necessarily has an exploratory character. Because the stability and orderliness of the supported behavior were unknown at the outset of the experiment, we exposed 8 birds to the procedures with VI schedules composed of exponential (Fleshler & Hoffman, 1962) distributions of interreinforcement intervals (IRI). A second set of 8 birds had rectangular IRI distributions. Our selections for Phase 1 were a VI 20-s schedule with T_{VI} of 200 s followed by 800 s of extinction, yielding a T_{trial} of 1,000 s. During Phase 2, we grouped the birds into sets of 4 and changed either the T_{VI} (200 s to 300 s) or the VI schedule (VI 20 s to VI 40 s) so we could test the predictions of linear analysis. T_{trial} was held constant for computational ease. The average number of reinforcers was determined by the trial duration and the VI schedule. The actual VI schedules were constructed with a sequence of IRI times that were exhaustively drawn, without replacement, from a randomized pool containing five sets of identical 20 element Fleshler–Hoffman or rectangular values (i.e., similar to a VI tape). Each experi-

mental session was begun at a random point in that fixed sequence of IRI times.

CONCEPTUAL FRAMEWORK AND AUXILIARY TECHNIQUES

Determining the quantitative relationship between the obtained structure in steady-state behavior and the supporting reinforcement schedule is the core of our linear analysis. There are two auxiliary techniques that are required to obtain and use this relationship— one specialized for repeated-trials data and the other quite general. We will cover these auxiliary techniques first and then subsequently address the framework used to predict behavior.

Averaged Steady-State Dynamics

This subsection defines the technique that we used to obtain an average steady state from the repeated-trials data. The characteristics of the average are briefly discussed. In addition, we will consider the resulting averages without reference to linear analysis.

We applied a technique, the *repeated-trials local average,* to both the input data (reinforcer delivery times) and the output data (operant response times) to combine the steady-state trials. This is a common technique used to compute the average behavior supported by a fixed-interval (FI) schedule: The within-trial elapsed time for a set of trials is first synchronized to a common time base and the resulting ensemble is then averaged. For this experiment's data reduction we used a common time base, T_{trial} in length, divided into 512 equal time subintervals, or bins. The reinforcement and response times from all trials after stability occurred (as noted, the final 20 sessions) were mapped to the common time base. We computed the local average rates of reinforcement and responding for each bin by dividing the number of events occurring in the bin by the time duration of that bin. The end result is the averaged moment-to-moment changes in the reinforcement rate and the response rate at each point in the trial interval. The choice of 512 bins was determined by the fast Fourier transform (FFT) routines used in the linear analysis.

A repeated-trials local average condenses the completely local (or molecular) snapshots of behavior or reinforcement from the individual trials into a single composite picture. To reach the more global time averages used in molar studies, one would continue condensing the data along the length of the common time-base interval by further averaging across the 512 bin rates to produce a single average rate. A repeated-trials local average is probably meaningful only after an organism has reached steady state. Furthermore, the obtained repeated-trials local average should not be confused with the first extinction exposure, just as the average steady-state FI scallop should not be confused with the initial acquisition.

Figure 2 shows data from 4 representative birds obtained during the steady-state portion of Phase 1. There is considerable precision in the control of responding during steady state by the duration of the VI schedule, T_{VI}, apparent in Figure 2. A similarly precise temporal control has been shown with the peak procedure (Catania, 1970; Roberts, 1981). The 200-s length for the VI schedule portion of the trial was invariant and was timed irrespective of the occurrences of responding or reinforcers, yet a noticeable change in response rate occurred within seconds of the actual T_{VI}. The well-defined falling edge seen in the behavior of the 4 birds in Figure 2 is not an artifact of averaging the steady-state trials and occurs in the data from 15 of the 16 birds. The standard deviation of the response rate does not noticeably increase for times close to T_{VI}, as would have occurred if the pigeons ceased responding over a range of times. The Phase 2 results showed similar precision in control of the behavior by the different VI schedules and T_{VI} durations.

The patterns of reinforcement and response rates are not completely featureless. There is local scatter in the reinforcement rates, which is a slight qualitative departure from the general overview of the schedule shown in Figure 1. Although the patterns of response rates are similar, each bird's repeated-trials local average behavior does show some unique characteristics.

Fourier Transforms

The Fourier transform is a standard mathematical technique often used as part of an analysis of time series data (Oppenheim & Schafer, 1975). It is particularly helpful when studying extended or intricate time depen-
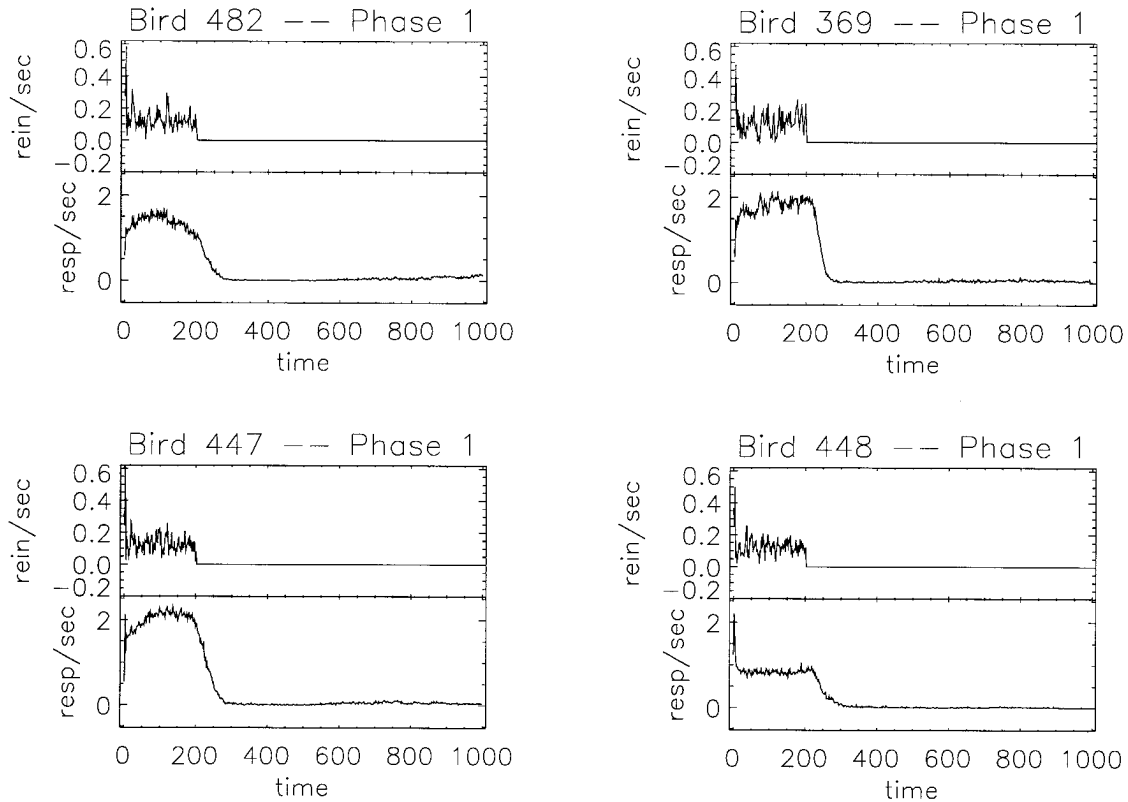
Fig. 2. Typical repeated-trials local average reinforcement (top frame of each panel) and supported behavior (bottom frame of each panel) for the Phase 1 step transition from a VI schedule to extinction. The left column shows data from the group with an exponential IRI distribution, and the right column shows data from the group with the rectangular IRI distribution. The scale of the scatter in reinforcement rates is compatible with the number of reinforcers delivered during the time used to compute the rate averages and $1/\sqrt{N}$ counting statistics.

dencies of an externally driven system. We will express the relationship between the reinforcement schedule and the supported behavior as a ratio of Fourier transforms. This subsection covers Fourier transform operations in general terms as well as the specific definition of the transform employed in this report.

A Fourier transform decomposes a function of time into a sum of sinusoidal (sine wave) components of different frequencies. The frequencies required in the sum to construct a given function are determined by the function. For example, an FI 20-s reinforcement schedule will have a strong component at 0.05 Hz (or 1/20 s). In general, a function that changes only slowly with time will be predominantly composed of low frequencies; a function that changes more rapidly will require a larger contribution from higher fre-

quencies. The sharp falling edge that appears in our experiment's reinforcement schedule will require high-frequency components to be significant in the Fourier transform. If a function of time contains structures at a time scale of Δt, the Fourier transform will contain significant components with frequencies that have half-cycle times that are at least as short as Δt (i.e., $f \geq 1/2\Delta t$). A sum of sinusoidal components can yield nonsinusoidal shapes: Even completely nonperiodic structures can be expressed by including the proper sinusoidal components in the sum.

With Fourier transforms we can isolate elements of the reinforcement schedule and its resulting behavior that vary on different time scales. If the behavior shows little variation over short time scales, then the Fourier transform will be small at higher frequencies, indicating that we can largely ignore these time

scales. In addition, this capability of Fourier transforms to separate by frequency makes possible the solution of an integral equation, central to our quantitative analysis, that otherwise is rather intractable.

As noted, the basic principle of the Fourier transform is that a very broad class of functions of time can be written as the sum of a possibly infinite number of sine and cosine functions. An identity called Euler's formula relates the complex exponential function with the sine and cosine functions: $e^{2\pi ift} = \cos 2\pi ft + i \sin 2\pi ft$. Using the complex exponential, the Fourier decomposition is expressed as a continuous summation of the form

$$H(t) = \int_{-\infty}^{\infty} h(f) e^{-2\pi ift} \, df, \qquad (1)$$

where $H(t)$ could be any function of time [e.g., $B(t)$ or $R(t')$ in Equation 3], and the function of frequency $h(f)$ is the amplitude of the sinusoidal component contributing to the sum at frequency f. In normal usage $h(f)$ is simply termed the Fourier transform of $H(t)$. An expression of similar form gives $h(f)$ in terms of $H(t)$:

$$h(f) = \int_{-\infty}^{\infty} H(t) e^{2\pi ift} \, dt. \qquad (2)$$

The two members of the $H(t)$, $h(f)$ pair are just different representations of the same information. The analytic definitions given in Equations 1 and 2 connect this pair of time- and frequency-domain functions. Equation 1 converts a function of frequency back to a function of time and is commonly termed the *back* or *inverse* Fourier transform. Similarly, Equation 2 converts a function of time to a function of frequency and is called the *forward* Fourier transform, or simply the Fourier transform.

The presence of negative frequencies in Equations 1 and 2 is a mathematical convenience. For the present experiment, the data has only real, as opposed to complex, values, and the Fourier transform could be defined without reference to negative frequencies. However, such a definition uses a somewhat nonstandard form that would raise other difficulties. The impact of using the standard form is that the negative frequencies will simply mirror the positive frequencies, as will be apparent in later figures.

Although Equations 1 and 2 are written in terms of continuous functions of time and frequency, $H(t)$ and $h(f)$, they have been implemented for discretely sampled data (such as the 512 bin values of the repeated-trials local averages) as a set of standard computer routines called fast Fourier transforms (FFTs). FFT routines are efficient, well tested, and reliable (see Press, Flannery, Teukolsky, & Vetterling, 1986, p. 381, for an extended discussion). Examples of the present experiment's time-domain data transformed to frequency-domain data with an FFT are given in the detailed analysis below.

The Fourier transform is one of several types of frequency transform. All concepts of linear analysis developed in prior work (e.g., McDowell et al., 1993) using the Laplace transform as the link between the time and frequency domains are the same. In fact, the Laplace transform can be derived as a special case of the Fourier transform (Mathews & Walker, 1965, p. 102).

Transfer Functions and the Prediction of Behavior

The quantitative relationship between reinforcement schedule and supported behavior given by the transfer function holds a central role in our efforts to predict behavior. This section covers how we use the transfer function, first to capture the relationship of the supported behavior to the reinforcement schedule seen in the Phase 1 data, then to predict the behavior supported in Phase 2 with a different reinforcement schedule. We implemented the analytic expressions that define this prediction in numerical form as part of our data-reduction software. We will work through these computational steps using a typical bird's data to provide a specific graphical example in the Results section below. The χ_v^2 measure for the fidelity of the prediction is also developed in the Results section.

When expressed as functions of time, the supported behavior at time t, $B(t)$, and the prior reinforcement schedule, $R(t')$, are related through linear analysis (McDowell et al., 1993) by the convolution integral

$$B(t) = \int_0^t G(t - t') R(t') \, dt'. \qquad (3)$$

The function $G(t - t')$ isolates the organism's contribution to the relationship of the supported behavior to the reinforcement schedule. In a behavioral experiment, $R(t')$ is determined by the experimenter, and $B(t)$ is the measured response. Thus, if Equation 3 can be solved for $G(t - t')$, it should be possible to predict the pigeon's response to a different reinforcement schedule. Phase 1 of this experiment is used to find the Fourier transform of $G(t - t')$, then Phase 2 is used to check the validity of the resulting prediction of behavior. (It is worth noting that $R(t)$ and $B(t)$ in the present work are repeated-trials local average rates, whereas in previous work a square pulse representation was used. Computing repeated-trials local averages for reinforcement and response rates will yield quantities that are equivalent to the value-like $R(t)$ and $B(t)$ previously used. One can assume that for this experiment all reinforcers have a common absolute magnitude and, similarly, all responses also have their own common absolute magnitude. Hence, these magnitudes will not affect the computations, and if a repeated-trials local average is computed, dividing by the length of the time bin results in dimensions of a local average rate.)

As discussed in prior work (McDowell et al., 1993), the standard method to simplify Equation 3 is by applying a frequency transform, so that Equation 3 becomes

$$b(f) = g(f) r(f), \qquad (4)$$

where $b(f)$, $g(f)$, and $r(f)$ are the Fourier transforms of $B(t)$, $G(t - t')$, and $R(t')$, respectively. In a relationship such as Equation 4 that describes the transformation of an input into a resulting output as functions of frequency, $g(f)$ is termed the *transfer function*.

Our data-reduction software uses Equation 4 in two somewhat different ways to bypass Equation 3. The major processing stages for both phases of the experiment are shown schematically in Figure 3. In each phase, the processing yields the boxed quantity.

Data from the first phase determine the transfer function, $g(f)$, for a specific subject. The three steps in the Phase 1 (p1) processing are:

1. Transform the measured reinforcement rate as a function of time, $R_{p1}(t)$, to the function of frequency, $r_{p1}(f)$.

2. Transform the measured response rate as a function of time, $B_{p1}(t)$, to the function of frequency, $b_{p1}(f)$.

3. From Equation 4, compute the transfer function as a function of frequency, $g(f)$, by division:

$$g(f) = \frac{b_{p1}(f)}{r_{p1}(f)}. \qquad (5)$$

If a linear analysis is appropriate for simple-schedule behavior, then the transfer function should isolate the characteristics of the specific organism under study and should not depend on the particular reinforcement input and response output used in its determination. The Phase 2 (p2) processing uses this assumed independence to predict the responding that ought to be seen with a new reinforcement schedule. There are again three steps in the processing:

1. Transform the measured reinforcement rate as a function of time, $R_{p2}(t)$, to the function of frequency, $r_{p2}(f)$.

2. Compute the predicted Phase 2 responding, $b_{p2}^{pred}(f)$, as a function of frequency using the transfer function, $g(f)$, obtained in Phase 1. The prediction is given by Equation 4:

$$b_{p2}^{pred}(f) = g(f) r_{p2}(f). \qquad (6)$$

3. Inverse transform the predicted response rate as a function of frequency, $b_{p2}^{pred}(f)$ to a function of time, $B_{p2}^{pred}(t)$, for comparison to the response rate actually measured, $B_{p2}(t)$.

It is important to note that $B_{p2}^{pred}(t)$ is an absolute prediction based solely on the Phase 1 measurement of $g(f)$ and the Phase 2 reinforcement schedule, $R_{p2}(t)$; no free (or adjustable) parameters are used in the prediction (beyond the determination of $g(f)$ in Phase 1).

There are technical points germane to our FFT-based data reduction that are, for the most part, more of interest to students of numerical analysis than of behavior analysis, so we simply note their existence here. They are dealt with in the Appendix, which presents a tutorial test case of linear analysis that is appropriate to the data-reduction problem at hand. Their chief effect is to produce spike artifacts in transfer functions computed with Equation 5. In general, the effects of these artifacts will not be important in the prediction of behavior because they occur mainly at higher frequencies and have random phases. The

Phase 1 processing for $g(f)$

Time Domain:

$$R_{p1}(t) \dashrightarrow \int_0^t G(t - t')R_{p1}(t')dt' = B_{p1}(t) \dashleftarrow B_{p1}(t)$$

FFT $\downarrow$ $\downarrow$ FFT

Frequency Domain:

$$r_{p1}(f) \longrightarrow \frac{b_{p1}(f)}{r_{p1}(f)} = \boxed{g(f)} \quad \longrightarrow b_{p1}(f)$$

Phase 2 processing for $B_{p2}^{pred}(t)$

Time Domain:

$$R_{p2}(t) \dashrightarrow \int_0^t G(t - t')R_{p2}(t')dt' = \boxed{B_{p2}^{pred}(t)} \longleftrightarrow B_{p2}(t)$$

FFT $\downarrow$ $\uparrow$ Inverse FFT

Frequency Domain:

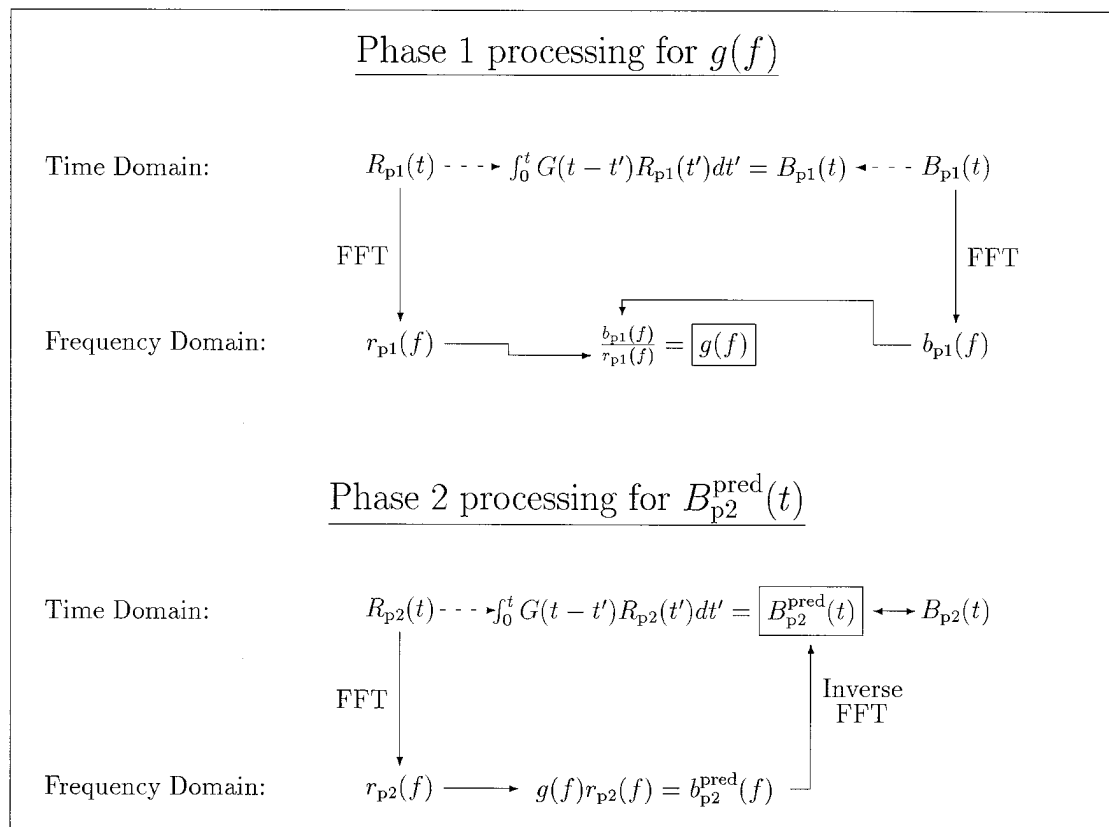$$r_{p2}(f) \longrightarrow g(f)r_{p2}(f) = b_{p2}^{pred}(f)$$

Fig. 3. Schematic diagram of the steps of the data processing (see text). Data from the first phase are used to determine the pigeon's transfer function, $g(f)$. Data from the second phase are used to predict the pigeon's behavior $B_{p2}^{pred}(t)$ and the prediction is compared to the measured behavior $B_{p2}(t)$. FFT routines provide the needed transformations between the time domain and the frequency domain and are shown as the vertical arrows labeled FFT and Inverse FFT.

important point for the reader to keep in mind is that although our data-reduction method is a sound means of extracting transfer functions, care is required in its actual use.

RESULTS

Bird 369: Step-by-Step Analysis and Intermediate Results

This subsection illustrates the data-reduction processing stages and displays the important intermediate results graphically for 1 of the 16 birds in this study. Bird 369 was selected as an example solely because it had the lowest serial number. With the exception of Bird 451 noted below, the data from any bird could have been used to illustrate the analysis. As discussed above and shown in Figure 3, the processing stages use Phase 1 reinforce-

ment and response data to extract a transfer function and then make a prediction of the Phase 2 responding.

The data reduction begins with collecting the reinforcement and response times from all trials after stability and computing the repeated-trials local averages for reinforcement and response rates. The reinforcement rate as a function of time, $R_{p1}(t)$, for Bird 369 is shown in the top frame of the upper right panel of Figure 2. The response rate as a function of time, $B_{p1}(t)$, for Bird 369 is shown in the lower frame of the same panel of Figure 2. Note that the scatter or noise in $B_{p1}(t)$ is relatively smaller than the scatter in $R_{p1}(t)$. Also note that the sharp edge in $R_{p1}(t)$ at the onset of extinction produces a softer falling edge in the bird's behavior seen in $B_{p1}(t)$.

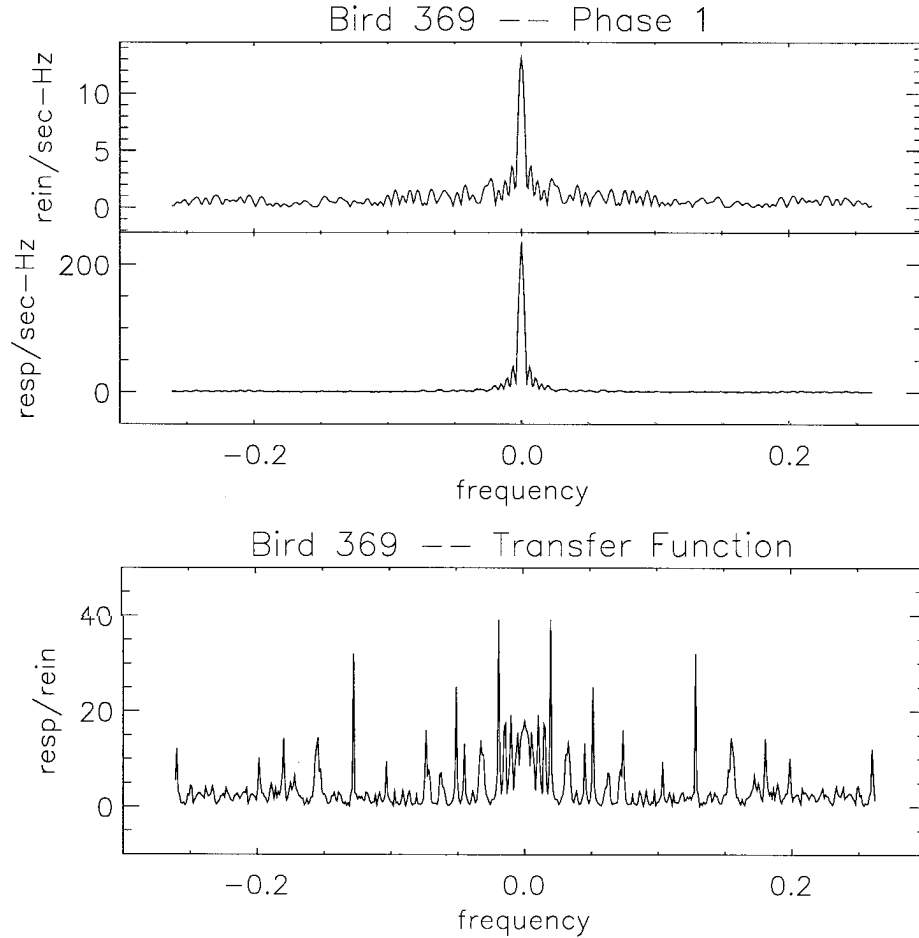The data from the experiment are discrete

Fig. 4. The Phase 1 results for Bird 369 displayed in the frequency domain and the amplitude of the resulting transfer function (see text). Note the expected symmetry about zero is apparent in $r(f)$, $b(f)$, and $g(f)$.

sets of rate samples over a finite time interval. This finite sampling resolution in the time domain is reflected in a corresponding finite sampling resolution in the frequency domain. The frequency scale produced by an FFT routine follows from the sampling rate employed. In this experiment, the trial length, T_{trial}, limits the lowest frequency component to

$$f_1 = \frac{1}{T_{\mathrm{trial}}}, \qquad (7)$$

or 1 mHz (1 mHz = 0.001 Hz) for the 1,000-s trials used. The highest frequency component is set by the Nyquist critical frequency, given by

$$f_c = \frac{1}{2\Delta}, \qquad (8)$$

where Δ is the time period between successive samples. Because the rates are computed for 512 time bins over the 1,000-s trials, the highest frequency components are at ±256 mHz. These two limits mean that in the frequency domain we can determine $r(f)$, $b(f)$, and $g(f)$ at frequencies of -255 mHz, -254 mHz, . . ., -1 mHz, 0 mHz, $+1$ mHz, $+2$ mHz, . . ., $+255$ mHz, $+256$ mHz. For further explanation of FFT routine frequency scales and Equations 7 and 8, please refer to Press et al. (1986).

The amplitude of the reinforcement rate as a function of frequency, $|r_{\mathrm{p1}}(f)|$, for Bird 369 is shown in the top panel of Figure 4. Because $|r_{\mathrm{p1}}(f)|$ is an amplitude per unit frequency range, the units are reinforcers per second-Hertz (or reinforcers per second divided by

Hertz). A frequency-domain phase plot also exists because $r_{p1}(f)$ is a complex function. The phase information is essential if one is actually doing the computations with Equation 5. For the discussion in this paper, however, the amplitude plots are sufficient. The form of $|r_{p1}(f)|$ is typical of an FFT for experimental data. The lower frequencies contain most of the meaningful structure of the data, and the higher frequencies have approximately equal amplitudes per frequency bin. To have equal amplitudes per frequency bin is characteristic of white noise; this region is termed the *noise floor* and is considered not to contain useful information. The low-frequency boundary of the noise floor for $|r_{p1}(f)|$ is not sharply defined, but begins no later than ± 100 mHz. The amplitude of the response rate as a function of frequency, $|b_{p1}(f)|$, for Bird 369 is shown in the middle panel of Figure 4. Comparing Bird 369's time-domain plots of Figure 2 and frequency-domain plots in Figure 4, one can see that the sharp edge at 200 s and the fast fluctuations in the reinforcement rate $R_{p1}(t)$ generate substantially greater amplitudes at higher frequencies[1] in $|r_{p1}(f)|$ than are generated in $|b_{p1}(f)|$ by the softer (slower) falling edge and steadier response rate of $B_{p1}(t)$.

By comparing the frequency-domain amplitude plots for Bird 369's reinforcement and response rates in Figure 4, one can see graphically the basic character of the transfer function. The behavior of Bird 369 is affected primarily by the low frequencies, rather than the higher frequencies, that are present in the input reinforcement. In the language of linear analysis, one would describe Bird 369 as operating as a form of low-pass filter.[2] Furthermore, all birds in this experiment have transfer functions with this same general low-pass character. These transfer functions allow prediction of the Phase 2 responding, in part, by quantifying how much each bird will filter out the higher frequencies.

The amplitude of the transfer function as a function of frequency, $|g(f)|$, for Bird 369 is shown in the bottom panel of Figure 4. For low frequencies, roughly $f \leq 30$ mHz, the transfer function is substantially larger than unity. These low-frequency values of the transfer function reflect that the pigeon's overall response rate (typically 2.5 responses per second) is faster than the reinforcement rate (typically 1 reinforcer per 20 s). The relative size of the transfer function at low frequencies compared to higher frequencies means that the resulting behavior is primarily a function of the longer time scales in the reinforcement schedule, such as the transition from VI to extinction that occurred once per 1,000 s. There are, however, many spikes in the higher frequency region. From Figure 4 one can see that these spikes occur mostly at frequencies for which both the reinforcement input and the response output amplitudes are determined mainly by noise. These spikes are generated at frequencies where $r_{p1}(f)$ is very small. The spikes will not greatly affect the prediction made with Equation 6, Because at these higher frequencies, $r_{p2}(f)$ will also be small. Still, one direction for future work will be reducing these effects of measurement noise on the computations.

With the measurement of the transfer function, $g(f)$, in hand, we can now predict the behavior that will be supported in steady state by a new schedule. We assigned Bird 369 to the Phase 2 test schedule group that had the same VI 20-s schedule and changed the step-transition time, T_{VI}, to 300 s. The experimentally measured repeated-trials local average response rate as a function of time, $B_{p2}(t)$, for Bird 369 during Phase 2 is shown in the top panel of Figure 5. The predicted response rate as a function of time during Phase 2, $B_{p2}^{pred}(t)$, found using the transfer function of Figure 4, is shown in the bottom panel of Figure 5. On the whole, the predicted behavior agrees with the measured behavior. (A χ_v^2 assessment of that agreement is presented below.)

The computation of the transfer function and prediction is the very simplest one could do. This prediction was made using $T_{trial} = 1,000$ s, which ignores the difficulties caused by the commensurate frequencies of zero amplitude discussed in the Appendix. No effort was made to reduce the effects of noise. In addition, there are time periods during which the bird is predicted to have an unattainable negative response rate. Iterative methods do

---

[1] The amplitude of $|r_{p1}(f)|$ is larger relative to the size of the zero frequency component spike than the amplitude of $|b_{p1}(f)|$ at most frequencies.

[2] There are many other types of low-pass filters beyond the simple resistor-capacitor low-pass filter discussed in the Appendix.
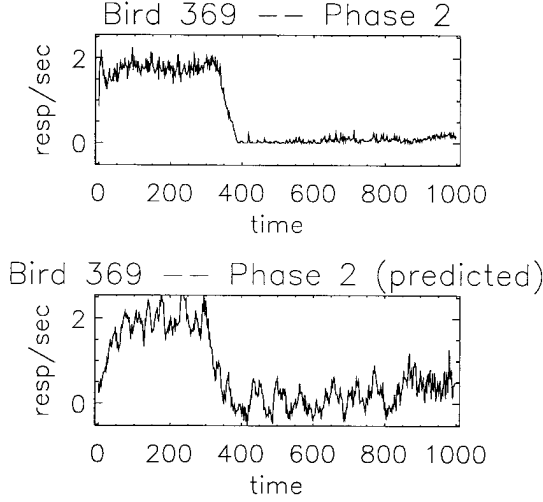
Fig. 5. The experimentally measured response rate as a function of time, $B_{p2}(t)$, for Bird 369 during Phase 2 is shown the top panel. The predicted response rate, $B_{p2}^{pred}(t)$, for Bird 369 during Phase 2 is shown in the bottom panel.

exist to constrain the transfer function, so responding is always greater than or equal to zero, but the implementation of such constraints would take us far afield.

χ_ν^2 *Measure and Overall Results*

We predicted the Phase 2 behavior for the remaining 15 birds with the same data-reduction routines we used on Bird 369's data. We also predicted the behavior for all 16 birds with the common time base length, T_{trial}, changed from 1,000 s to 977.11 s (the rationale for the second value of T_{trial} is given in the Appendix). Currently, no other analyses make predictions for the detailed steady-state form of $B(t)$. Hence, we are limited in quantitative evaluation of the results to measuring the discrepancy from a perfect prediction, that is, the discrepancy from the real observed Phase 2 data.

As a global measure of our Phase 2 predictions' accuracy, we used χ_ν^2, the reduced χ^2 of the discrepancy between $B_{p2}^{pred}(t)$, the linear system prediction, and $B_{p2}(t)$, the pigeon's measured responding. The expression for χ_ν^2 is given in this case by (Bevington, 1969, p. 187)

$$\chi_\nu^2 = \frac{1}{N} \sum_{i=1}^{N} \frac{1}{\sigma_{B_{p2,i}}^2} [B_{p2}(t_i) - B_{p2}^{pred}(t_i)]^2, \quad (9)$$

where $\sigma_{B_{p2,i}}^2$ is the variance in the ith measured Phase 2 response rate, $B_{p2}(t_i)$. Estimating $\sigma_{B_{p2,i}}^2$ during extinction is problematic because the response rate is so low that some of the time intervals contain no responses for any trial, leading to $B_{p2}(t_i) \equiv 0$ and $\sigma_{B_{p2,i}}^2 \equiv 0$. A reasonable estimate of the variance during the extinction interval is $\overline{\sigma_{B_{p2,EXT}}^2}$, the average of those actually measured (including those of zero value). Thus the expression used for χ_ν^2 becomes

$$\chi_\nu^2 = \frac{1}{N} \left\{ \sum_{i=1}^{M} \frac{1}{\sigma_{B_{p2,i}}^2} [B_{p2}(t_i) - B_{p2}^{pred}(t_i)]^2 \right.$$
$$\left. + \sum_{i=M+1}^{N} \frac{1}{\overline{\sigma_{B_{p2,EXT}}^2}} [B_{p2}(t_i) - B_{p2}^{pred}(t_i)]^2 \right\},$$
$$(10)$$

where t_M is the time closest to the onset of extinction at T_{VI}. Note that the normalizing factor that appears in Equation 10 is $1/N$ because there are no free parameters in $B_{p2}^{pred}(t)$. Hence, the number of degrees of freedom is equal to the number of data points.

The values of χ_ν^2 for all birds in this study are shown in Table 1 computed both with T_{trial} at the full 1,000 s and at 977.11 s. Because both Equations 9 and 10 are measures of a prediction's discrepancy, the lower the value of χ_ν^2, the better the quality of the prediction. The χ_ν^2 values specify the probability that a random (or chance) prediction could be as close to the data as our prediction. The distribution of χ_ν^2 values was noticeably bimodal. In the majority of cases, agreement between the actual Phase 2 responding and our prediction is better than chance for a $p < .01$ threshold. (For $N = 512$, the agreement between the predicted and obtained behavior occurs by chance less than one time in 100 when the χ_ν^2 is less than 0.8603.) When the prediction failed, the values of χ_ν^2 were at the other extreme. (The agreement between the predicted and obtained behavior occurs by chance at least 99 times in 100 when the χ_ν^2 is greater than 1.1511.)

The reader should be mindful that Equation 10 measures the overall quality of the prediction. There are smaller features in most birds' Phase 2 responding that are not accurately predicted. Even so, the fidelity to

Table 1

The values of χ_ν^2 for the birds in this study.

Bird	χ_ν^2 (1,000 s)	χ_ν^2 (977.11 s)
Phase 1 Fleshler–Hoffman: VI 20, T_{VI} = 200 s		
Phase 2 Fleshler–Hoffman: VI 40, T_{VI} = 300 s		
424	0.4791	0.5601
467	0.3615	0.4892
468	1.1792	1.3879
482	0.4280	0.4865
Phase 1 Fleshler–Hoffman: VI 20, T_{VI} = 200 s		
Phase 2 Fleshler–Hoffman: VI 40, T_{VI} = 200 s		
447	0.6110	0.2627
460	0.2779	0.4455
461	1.0350	0.9656
475	0.2794	0.2826
Phase 1 rectangular: VI 20, T_{VI} = 200 s		
Phase 2 rectangular: VI 20, T_{VI} = 300 s		
369	0.5880	1.3112
438	10.1653	2.1843
445	1.4199	0.5767
451	1.0879	0.9083
Phase 1 rectangular: VI 20, T_{VI} = 200 s		
Phase 2 rectangular: VI 40, T_{VI} = 200 s		
426	0.4322	0.9747
448	1.5433	2.4711
454	0.3737	0.3904
488	3.3400	3.5335

Note. T_{VI} indicates the length of time during the trial that the VI schedule was in effect.
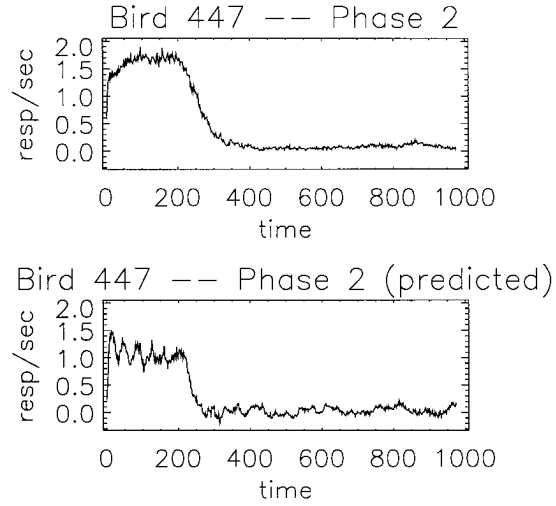

Fig. 6.　The experimentally measured response rate as a function of time, $B_{p2}(t)$, for Bird 447 during Phase 2 is shown the top panel. Note that the data set has been truncated slightly so T_{trial} = 977.11 s (see Appendix). The predicted response rate, $B_{p2}^{pred}(t)$, for Bird 447 during Phase 2 is shown in the bottom panel.

observed detail in the measured behavior by predicted behavior can be reasonably good. As an example, Figure 6 shows the measured and predicted Phase 2 responding of Bird 447. Also note that a bird's transfer function is unique to that specific bird. For example, the best Phase 2 prediction (lowest χ_ν^2) for Bird 369 is made with Bird 369's own transfer function.

In most cases in which the prediction was unsatisfactory, the difficulties could be traced to a processing artifact that occurs in Equation 5. As has been noted and is discussed further in the Appendix, at some frequencies the amplitude of $r_{p1}(f)$ can be quite small and can result in a narrow spike in the transfer function. The data from Bird 488 provide a good illustration of the artifact and its effect on the prediction. The top panel of Figure 7 shows the amplitude of the transfer function. Note the large spikes at ±10 mHz. The bottom panel of Figure 7 shows the predicted Phase 2 behavior. A large 10-mHz oscillation is clearly apparent in the prediction. Howev-

er, if we remove the most serious spike artifacts by replacing the values $g(f)$ with nearest neighbor averages at the ±10-mHz and ±5-mHz spikes, we reduce the discrepancy between the predicted and the obtained behavior. The revised prediction had a χ_ν^2 of 1.2023, improved by roughly a factor of three. There are more formal and mathematically rigorous methods to correct for such spike artifacts, but clearly the entire problem can be simply avoided. In future experiments, the schedule of reinforcement used in the measurement of the transfer function should be selected so that the amplitude of $r_{p1}(f)$ is significantly greater than zero in the frequency region of interest.

The response pattern of 1 of the birds, Bird 451, was unique and caused the data reduction and prediction methods to fail in an interesting manner. The Phase 1 reinforcement and responding are shown in Figure 8. Unlike all other birds in this study, Bird 451 responded at a relatively high rate throughout T_{trial} (including the entire 800-s extinction period). This violates a restriction of our FFT-based computation. Recall from Equation 7 that the lowest nonzero frequency component that the FFT will determine is for the frequency $1/T_{trial}$. In the case of Bird 451, the behavior in the time domain would have con-
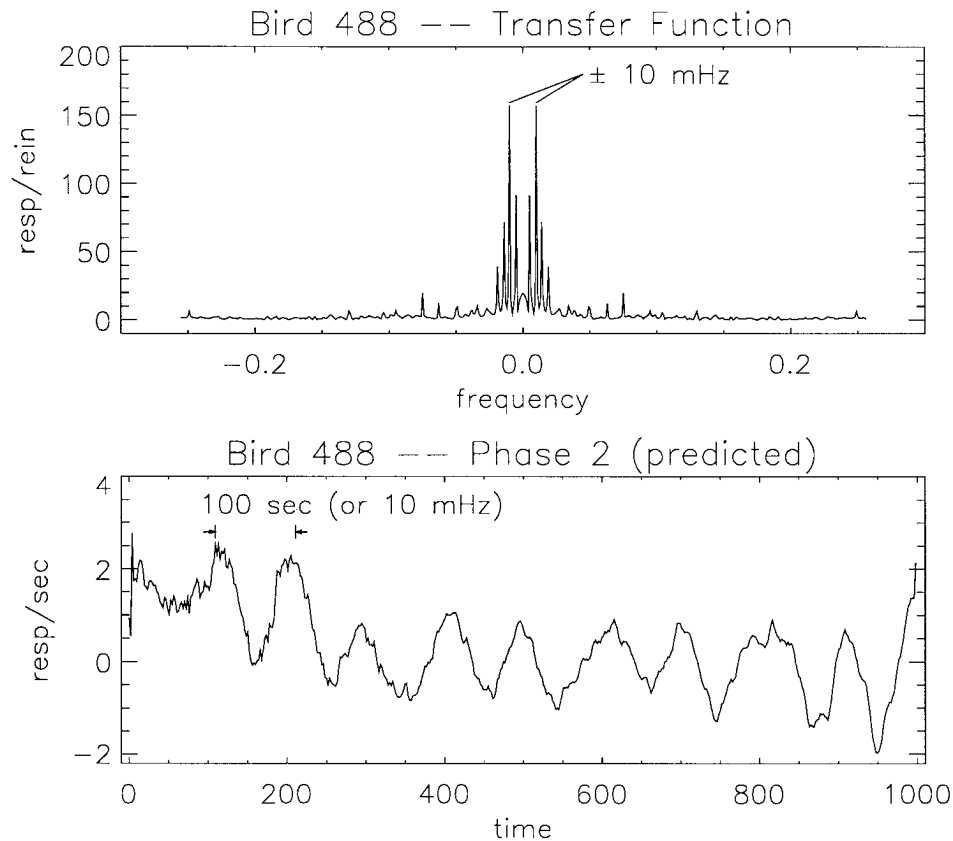
Fig. 7. The amplitude of the transfer function, $|g(f)|$, for Bird 488 is shown the top panel. The predicted response rate, $B_{p2}(t)$, for Bird 488 during Phase 2 is shown in the bottom panel.
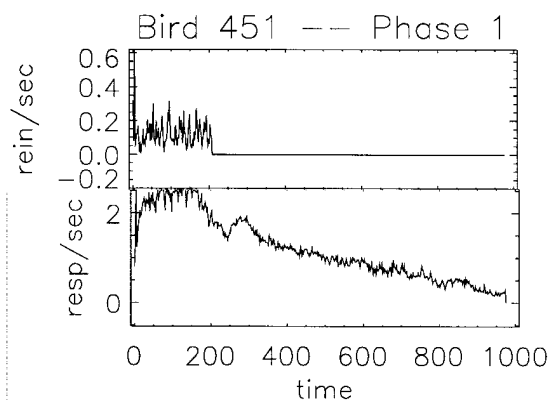

Fig. 8. The experimentally measured reinforcement rate as a function of time, $R_{p1}(t)$, for Bird 451 during Phase 1 is shown in the top panel. The measured response rate, $B_{p1}(t)$, for Bird 451 during Phase 1 is shown in the bottom panel. Compare this bird's response pattern to those of Bird 369 (Figures 2 or 5), Bird 447 (Figure 6), or any of the other birds shown in Figure 2.

tinued during extinction for a longer time than the limit imposed by T_{trial}. Hence, in the frequency domain there are behaviorally important frequency components below the $1/T_{trial}$ limit. Because the FFT excludes these lower frequencies from the computations, the prediction does not agree with the measured Phase 2 behavior to any significant extent.

DISCUSSION

The conclusions that can be drawn from this study are that (a) the general qualitative form for pigeons' transfer functions is that of a low-pass filter, and (b) using the experimentally measured transfer function allows some predictability of the pigeons' behavior under a different set of contingencies. The present experiment is the first effort to extract a transfer function from experimental data and the first to use a linear analysis to

predict behavior dynamics, albeit in a repeated-trials local average steady state. The values of χ^2_v are reasonably good for a prediction without free parameters, suggesting at least some measure of confidence in the application of linear analysis to behavior. Whether other methods, linear or not, can make comparable or superior predictions of future dynamic behavior based on prior experimental observations remains an open question.

A variety of past work has sought to characterize a reductionistic process that could result in the functional properties obtained between temporal requirements and obtained behavior. These efforts are exemplified by a number of models based on internal pacemakers (Church, 1984; Gibbon, 1991; Killeen, 1991). In contrast, the transfer function provides a quantitative method to capture an external view of the empirical relationship between the temporal properties of environmental contingencies and the supported behavior. Consequently, our analysis is silent on an internal view and does not distinguish or contradict the various timing models. However, should one of these models of timing be recast for application to our experimental procedure, a prediction of low-pass behavior must fall out naturally. In addition, our experiment is silent on the mechanism that causes short IRI distributions to be preferred. The low-pass character applies to the overall dynamic structure of the trial.

Based on the results of this experiment, one can now refine the measurement of a steady-state transfer function, and more demanding tests can be designed. From the standpoint of linear analysis, this experiment's results, particularly the low-pass character of the transfer function and the existence of computational spike artifacts, provide important guideposts for improvement. In future work, the reinforcement schedule should permit more detailed study of the lower frequency domain (i.e., frequencies of roughly ±150 mHz). The reinforcement schedule will also have to be carefully chosen to prevent the occurrence of zero or near-zero amplitudes within this behaviorally significant frequency domain.

REFERENCES

Anderson, L. W., & Beeman, W. W. (1973). *Electric circuits and modern electronics* (pp. 137–138). New York: Holt, Rinehart and Winston.

Baum, W. M. (1979). Matching, undermatching, and overmatching in studies of choice. *Journal of the Experimental Analysis of Behavior, 32,* 269–281.

Bevington, P. R. (1969). *Data reduction and error analysis for the physical sciences.* New York: McGraw-Hill.

Catania, A. C. (1970). Reinforcement schedules and psychophysical judgments: A study of some temporal properties of behavior. In W. N. Schoenfeld (Ed.), *The theory of reinforcement schedules* (pp. 1–42). New York: Appleton-Century-Crofts.

Church, R. M. (1984). Properties of the internal clock. In J. Gibbon & L. Allen (Eds.), *Timing and time perception* (pp. 566–582). New York: New York Academy of Sciences.

Fleshler, M., & Hoffman, H. S. (1962). A progression for generating variable-interval schedules. *Journal of the Experimental Analysis of Behavior, 5,* 529–530.

Galbicka, G. (in press). Rate and the analysis of behavior: Time to move forward? In L. J. Hayes & P. M. Ghezzi (Eds.), *Investigations in behavioral epistemology.* Reno, NV: Context Press.

Galbicka, G., Kautz, M. A., & Jagers, T. (1993). Response acquisition under targeted percentile schedules: A continuing quandary for molar models of operant behavior. *Journal of the Experimental Analysis of Behavior, 60,* 171–184.

Gibbon, J. (1991). Origins of scalar timing. *Learning and Motivation, 22,* 3–38.

Killeen, P. R. (1991). Behavior's time. In G. H. Bower (Eds.), *The psychology of learning and motivation* (pp. 295–334). New York: Academic Press.

Mathews, J., & Walker, R. L. (1965). *Mathematical methods of physics.* New York: W. A. Benjamin.

McDowell, J. J, Bass, R., & Kessel, R. (1992). Applying linear systems analysis to dynamic behavior. *Journal of the Experimental Analysis of Behavior, 57,* 377–391.

McDowell, J. J, Bass, R., & Kessel, R. (1993). A new understanding of the foundation of linear system theory and an extension to nonlinear cases. *Psychological Review, 100,* 407–419.

Oppenheim, A. V., & Schafer, R. W. (1975). *Digital signal processing.* Englewood Cliffs, NJ: Prentice Hall.

Palya, W. L., & Walter, D. E. (1993). A powerful, inexpensive experiment controller or IBM PC interface and experiment control language. *Behavior Research Methods, Instruments, & Computers, 25,* 127–136.

Press, W. H., Flannery, B. P., Teukolsky, S. A., & Vetterling, W. T. (1986). *Numerical recipes the art of scientific computing.* Cambridge: Cambridge University Press.

Roberts, S. (1981). Isolation of an internal clock. *Journal of Experimental Psychology: Animal Behavior Processes, 7,* 242–268.

APPENDIX

Computation of a transfer function by dividing two FFTs, as is done by Equation 5, does introduce some artifacts into the data processing. Such difficulties with divisions are fairly standard in frequency-domain work, because many time-domain functions yield frequency-domain functions with zero amplitude for some particular frequencies and/or for all frequencies higher than some cut-off frequency. Thus, $r(f)$ can easily be zero (or very close to it) for a range of frequencies, and Equation 5 cannot be evaluated within this range. For an ideal linear system, $b(f)$ would also be zero at these frequencies and result in the indeterminate expression of $0/0$ for $g(f)$. This problem is exacerbated by the fact that computer FFT algorithms do not perform true Fourier transforms over a continuum of frequencies, but instead perform a discrete Fourier transform (DFT): an approximation using a discrete set of frequencies (Oppenheim & Schafer, 1975; Press et al., 1986). As will be shown below, the sharp step from a static VI schedule to a period of extinction in the time domain can produce a discrete set of frequencies at which $r(f) = 0$.

A test case will illustrate the use of FFT-based routines to solve a linear analysis problem and provide some insight into the technique's stability and limitations. Unlike the behavior of a pigeon, we have an excellent theoretical model for the behavior of the electrical circuit used as the test case. As a result, we are able to compare the transfer function found by division of output by input with the correct transfer function. We shall see how the problems, primarily noise and zero-amplitude frequencies, introduce spike artifacts into the computed transfer function. We should expect the same effects to appear in any real data of similar form.

This test case is a standard low-pass electrical filter normally built with a resistor and capacitor in series and commonly referred to as an *RC low-pass filter*. The circuit is shown in Figure 9. Extended discussion of this circuit can be found in most basic electrical circuits textbooks (e.g., Anderson & Beeman, 1973, p. 137). The most important point about this circuit for the present discussion is that it is completely linear. This means that an expres-
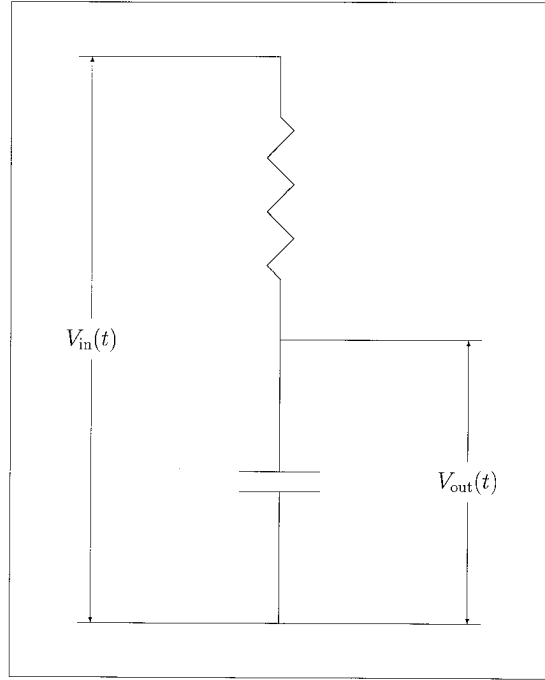

Fig. 9. A resistor-capacitor (RC) low-pass filter. The characteristic time constant of such a filter is given by $\tau = RC$. $V_{in}(t)$ and $V_{out}(t)$ indicate the input and output voltages as functions of time.

sion of Equation 3's form relates the output voltage to the input voltage:

$$V_{out}(t) = \int_0^t G_{RC}(t - t') V_{in}(t') \, dt'. \quad (11)$$

In the frequency domain the voltages are related by

$$v_{out}(f) = g_{RC}(f) v_{in}(f). \quad (12)$$

Beyond satisfying the general relations of Equations 11 and 12, an RC low-pass filter is a convenient test case because closed-form analytic expressions exist for both $g_{RC}(f)$ and a $V_{in}(t)$, $V_{out}(t)$ pair.

Commensurate Frequencies of Zero Amplitude

We will begin with a $V_{in}(t)$, $V_{out}(t)$ pair that is reasonably similar to the $R(t)$, $B(t)$ pairs observed in the actual data of this study.

We choose the input voltage shown in the top panel of Figure 10. The analytic expression for a square step in the time domain is
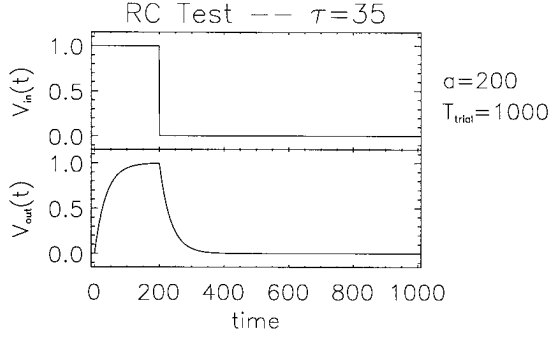
Fig. 10.   A square step input voltage (V_{in}) is shown in the top panel. The bottom panel shows the output voltage (V_{out}) from the circuit shown in Figure 9.

$$V_{in}(t) = \begin{cases} 1 & 0 \le t \le a \\ 0 & a < t \end{cases}. \qquad (13)$$

The output voltage generated by an RC low-pass filter in response to the input square step given by Equation 13 is

$$V_{out}(t) = \begin{cases} 1 - e^{-t/\tau} & 0 \le t \le a \\ e^{-(t-a)/\tau} & a < t \end{cases} \qquad (14)$$

and is shown in the bottom panel of Figure 10.

The analytic expression for the transfer function of an RC low-pass filter is

$$g_{RC}(f) = e^{i\phi} \frac{1}{\sqrt{1 + \left(\dfrac{f}{f_\circ}\right)^2}}, \qquad (15)$$

where the phase angle is

$$\phi = \arctan \frac{f}{f_\circ}, \qquad (16)$$

and the filter's critical frequency, $f_\circ$, is a characteristic of the filter related to its time constant, $\tau = RC$, by

$$f_\circ = \frac{1}{2\pi\tau}. \qquad (17)$$

The transfer function's amplitude, $|g_{RC}(f)|$, computed with Equation 15, is shown in the top panel of Figure 11.

Equations 13 and 14 provide an input–output pair in the correct form to run through the Phase 1 processing described in the text and shown schematically in Figure 3. Accord-

ingly, the middle panel of Figure 11 shows the $|g_{RC}(f)|$ that results when the $V_{in}(t)$, $V_{out}(t)$ pair shown in Figure 10, which has $a = 200$, $T_{trial} = 1,000$, and $\tau = 35$, is run through the data-reduction software. The disagreement between the actual and computed RC low-pass transfer functions is apparent and illustrative of the problems encountered in reducing the data from our experiment. When Equation 13 is transformed into the frequency domain with Equation 2, one obtains

$$v_{in}(f) = e^{2\pi i f a/2} \left[\frac{\sin(2\pi f a/2)}{2\pi f} \right]. \qquad (18)$$

Note that for nonzero frequencies, the factor $\sin(2\pi f a/2)$ will cause $v_{in}(f)$ to be zero if fa is an integer. If $a = 200$ and $T_{trial} = 1,000$, fa is exactly an integer at $f = \pm 5$ mHz, ± 10 mHz, ± 15 mHz, . . ., and so forth. Note that $v_{out}(f)$, the Fourier transform of $V_{out}(t)$, is, from Equation 12, also zero at these frequencies. The significance to our data reduction is that, in an unanticipated mathematical coincidence (caused by selecting a value of T_{VI} that is a simple rational fraction of T_{trial}, e.g., 1/5 for Phase 1), these same frequencies are used, because of the discrete Fourier transform, to evaluate Equation 5. This accounts for the large artifacts at every fifth frequency shown in the middle panel of Figure 11. At the remaining frequencies, the transfer function values computed by the data-reduction software agree, within machine precision, to the correct values calculated directly with Equation 15.

As a simple refinement to the data reduction that avoids this problem of commensurate frequencies of zero amplitude, we can exclude a small interval from the end of the trial. This introduces a slight offset between all the FFT component frequencies defined by Equation 7 and the zeros of Equation 18. To generate this offset, we arbitrarily chose $T_{trial} = 977.11$ s and ignored the data from the last 22.89 s of each 1,000-s trial. The bottom panel of Figure 11 shows the $|g_{RC}(f)|$ that results for a $V_{in}(t)$, $V_{out}(t)$ pair that has $a = 200$, $T_{trial} = 977.11$, and $\tau = 35$. The change in the FFT routine frequency scale obtained by changing T_{trial} is small, 2.3% in f_1, but it is sufficient to avoid the zero-amplitude frequencies when fa is an integer. As a result, the transfer function computed from this
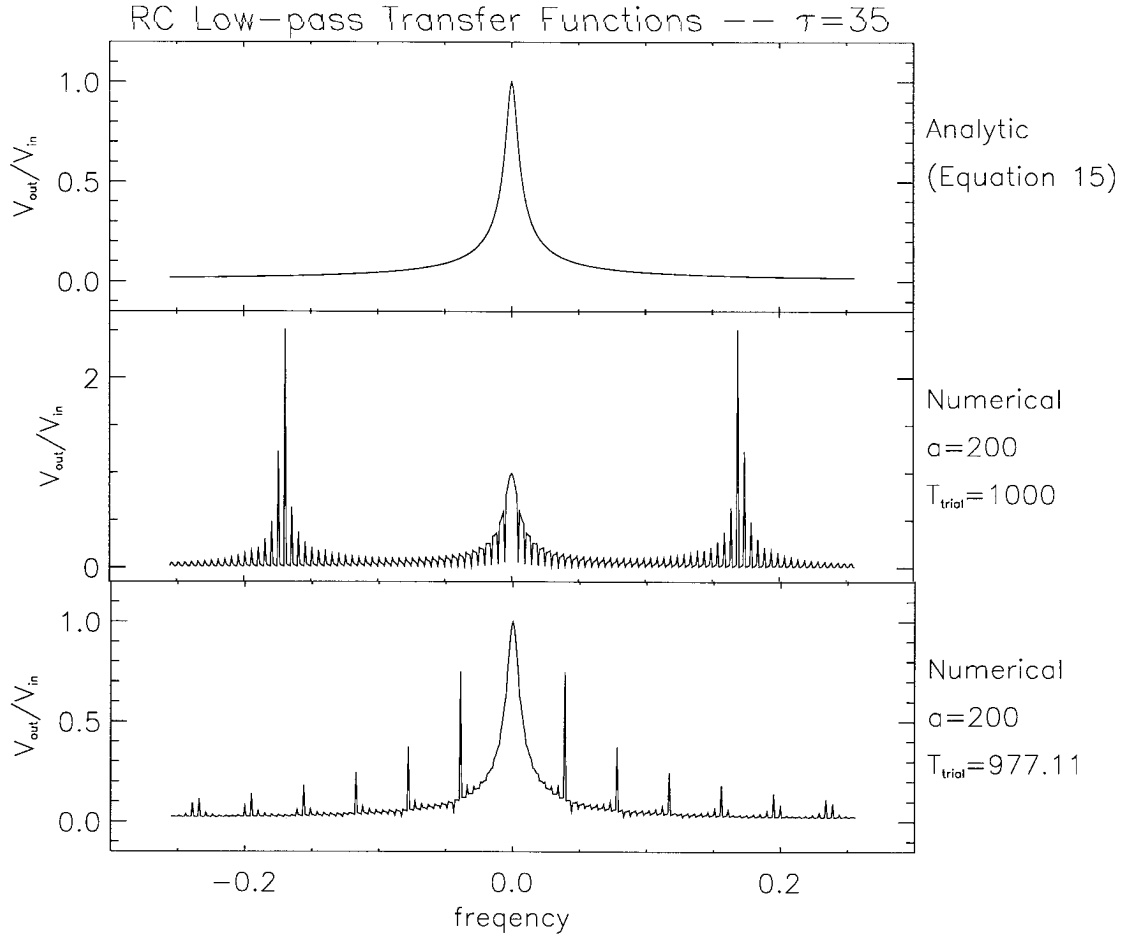
Fig. 11.   The top panel shows the transfer function of an RC low-pass filter as computed directly from the circuit's electrical properties. The middle panel shows the transfer function computed with discretely sampled values from Equations 13 and 14, where $a = 200$ and $T_{\text{trial}} = 1,000$. The bottom panel shows the transfer function computed with discretely sampled values from Equations 13 and 14, but where $a = 200$ and $T_{\text{trial}} = 977.11$.

$V_{\text{in}}(t)$, $V_{\text{out}}(t)$ pair agrees closely with the correct transfer function shown in the top panel. However, there are still some frequencies that, although not exactly commensurate with a zero-amplitude frequency, are quite close to these frequencies. At such frequencies, which occur roughly every 45 mHz, the transfer function is improperly determined.

Impact of Noise

Across a broad band of the higher frequencies measured in this experiment, the amplitudes of both $r(f)$ and $b(f)$ are small and are dominated by random noise. The noise has the minor advantage that the actual occurrence of a zero denominator (discussed above) almost never happens, but, obviously, the computed $g(f)$ will not be reliable when either the numerator or denominator in Equation 5 is dominated by noise. The ultimate effect is that the predicted Phase 2 responding will always be noisier than the actual data.

One can accurately simulate experimental data that contain noise (rapid uncorrelated fluctuations) and use the RC low-pass filter test case to study how noise limits the method's resolution. The overall result of these tests is that the resolution of our data-reduction method decreases as the noise increases.

Figure 12 shows a $V_{\text{in}}(t)$, $V_{\text{out}}(t)$ pair to which we have added a moderate amount of
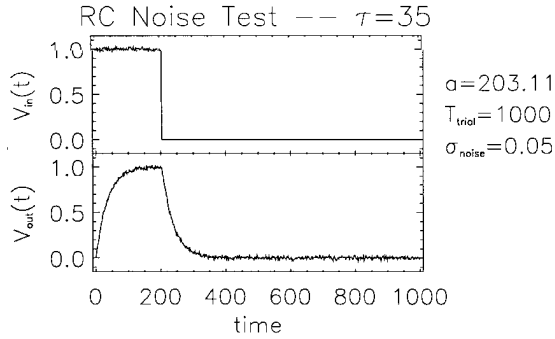
Fig. 12.   The top panel shows an input to an RC low-pass filter with Gaussian noise added. The bottom panel shows an output from an RC low-pass filter with Gaussian noise added.

Gaussian-distributed random noise. To mimic the experiment's reinforcement data, the $V_{in}(t)$ shown in Figure 12 has no added noise during the period corresponding to extinction in the actual experiment. We found, somewhat counterintuitively, that removing the noise from this portion of the input increases the data-reduction software's sensitivity to noise.

Figure 13 shows the results generated by our data-reduction software when the $V_{in}(t)$, $V_{out}(t)$ pair from Figure 12 is used to compute a transfer function, $g_{RC,noise}(f)$. The top panel shows the amplitude of the transfer function, $|g_{RC,noise}(f)|$. Although the low-frequency values of the transfer function are faithful to $|g_{RC}(f)|$, for frequencies beyond ±50 mHz the noise causes large spikes in the transfer func-
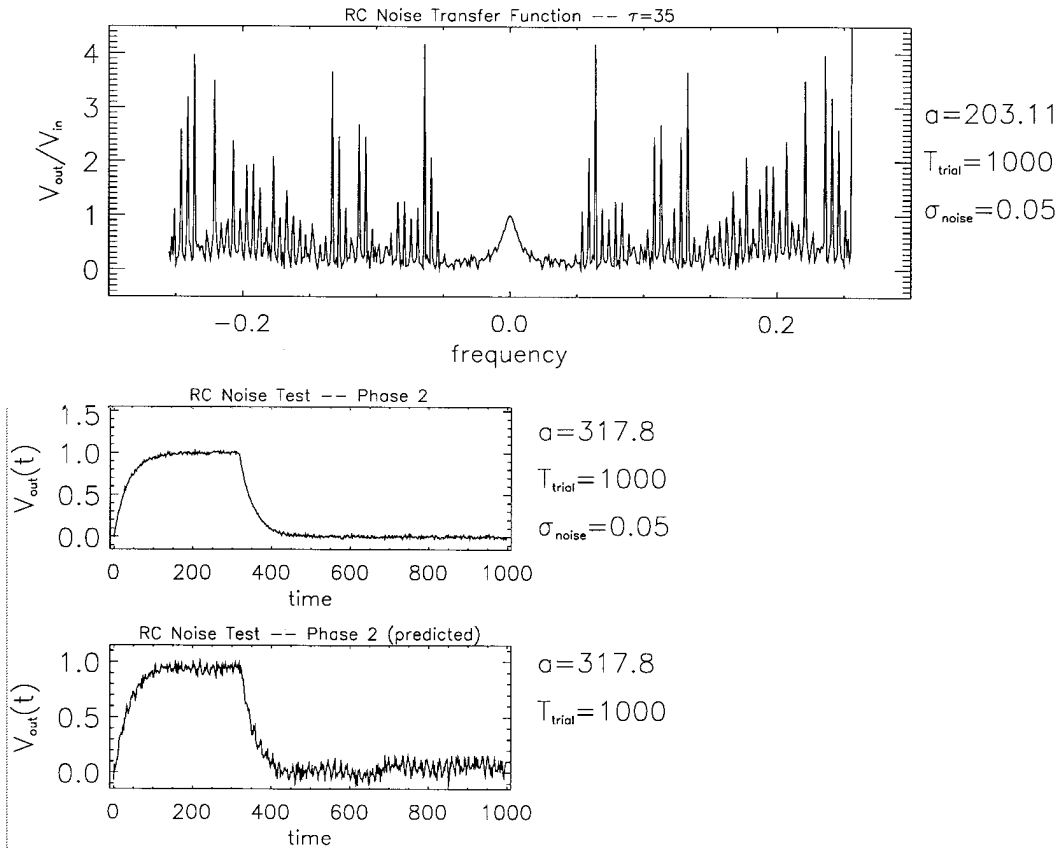

Fig. 13.   Results generated by our data-reduction software when the $V_{in}(t)$, $V_{out}(t)$ pair from Figure 12 is used. The top panel shows the amplitude of the transfer function as a function of frequency, $|g_{RC,noise}(f)|$. The middle panel is an output voltage computed directly from the circuit's electrical properties with an appropriate noise envelope $V_{out,noise}(t)$. The bottom panel shows predicted output voltage as a function of time, $V_{out,noise}^{pred}(t)$, computed with the derived transfer function. Note that the bottom two panels of this figure are functions of time, whereas the top panel is a function of frequency.

tion. As one increases the noise amplitude, these spikes appear at lower frequencies. The middle panel shows an output voltage computed directly from the circuit's electrical properties when the input step lasts for 317.8 s instead of 203.11 s with a noise addition: $V_{\text{out,noise}}(t)$. The bottom panel shows the predicted output voltage, $V_{\text{out,noise}}^{\text{pred}}(t)$, computed with the derived transfer function, $g_{\text{RC,noise}}(f)$.

Because both $V_{\text{in}}(t)$ and $V_{\text{out}}(t)$ have noise, it should not be surprising that the prediction will have more noise than either one. The di-

vision in Equation 5 will increase the relative noise amplitude on average by a factor of about $\sqrt{2}$ for the lower frequencies when noise is not, in general, a substantial problem. At higher frequencies when the noise-free amplitudes for $v_{\text{in}}(f)$ and $v_{\text{out}}(f)$ are small, the noise contribution to $g_{\text{RC,noise}}(f)$ will dominate. A possible refinement of the data reduction would be smoothing of these high-frequency spikes. Finally, during the evaluation of Equation 6, a second increase in relative noise amplitude will occur.